Industrial Crops & Products 166 (2021) 113475

Contents lists available at ScienceDirect

Industrial Crops & Products

journal homepage: www.elsevier.com/locate/indcrop

Quantitative analysis of feedstock structural properties can help to produce willow biochar with homogenous pore system

Kimmo Rasa [a,*], Anneli Viherä-Aarnio [b], Peetu Rytkönen [c], Jari Hyväluoma [d], Janne Kaseva [a], Heikki Suhonen [e], Tuula Jyske [c]

[a] Natural Resources Institute Finland (Luke), Tietotie 4, 31600, Jokioinen, Finland
[b] Natural Resources Institute Finland (Luke), Latokartanonkaari 9, 00790, Helsinki, Finland
[c] Natural Resources Institute Finland (Luke), Tietotie 2, 02150, Espoo, Finland
[d] Häme University of Applied Sciences (HAMK), Mustialantie 105, 31310, Mustiala, Finland
[e] Department of Physics, University of Helsinki, PL 64, 00014, Helsinki, Finland

ARTICLE INFO

Keywords:
Salix
Biochar
3D imaging
X-ray tomography
Pore structure
Wood structure
Vessels
Fibres

ABSTRACT

Novel bioeconomic approaches call for increasingly faster production of lignocellulosic biomass and its better-tailored use for higher added value. The high-yield capacity and structural properties of willows (*Salix* spp.) suggest their excellent potential for the production of designed biochar for use in agronomic, electronic and technical applications. All these applications rely on the internal pore structure of biochar. However, we lack an in-depth quantitative understanding of the interlinkages between the feedstock properties and the physical quality of the biochar produced. We studied quantitatively how the clonal and within-plant properties of five different willow clones (hybrids of *Salix schwerinii* E.L. Wolf) affected the micrometre-scale pore properties of the produced biochars (pyrolyzed at + 462 °C). The porosity and pore size distribution were analysed before and after slow pyrolysis by X-ray microtomography and image analysis. We also studied the potential of conventional low-cost fibre analysis techniques to be used to predict biochar pore properties directly from fresh feedstock. The total porosity (0.55–0.62) and the pore size distribution of willow wood and derived biochars varied between clones. Approximately two-thirds of the biochar total porosity was associated with pores formed by wood fibres. Pyrolysis levelled off the structural variation detected between and within the clones. Pyrolysis-induced shrinkage reduced the pore sizes and narrowed the pore size distribution. The results suggest that conventional fibre analysis techniques could be utilized to predict biochar homogeneity. Short rotation coppice willows are suitable feedstock to produce homogenous biochar precursor for production of bio-based carbon materials to be used in high value-added technical applications. The structural homogeneity of the feedstock and produced biochar can be enhanced by selecting proper harvesting strategy and clones used in plantations. From the industrial perspective, comprehensive understanding of feedstock properties helps to control quality of the produced biochar.

1. Introduction

Biochar is a solid end-product from the slow pyrolysis process. The pyrolysis process converts biomass-bound carbon towards aromatic structures, making it highly resistant against biological decomposition. In addition to carbon sequestration potential, the most distinguished feature of biochar is its porous structure capable of storing and transporting fluids and retaining dissolved and suspended solids. Biochar applications relying on internal porosity range from high quantity use in soils and growing media (Brassard et al., 2016; Lehmann et al., 2011; Turunen et al., 2020) to many proposed higher value-added non-soil applications (Bartoli et al., 2020), where the quality of biochar is of importance. For example, biochars can be used to replace non-renewable materials in applications such as activated carbons used in water and gas purification (Siipola et al., 2018), additives to enhance anaerobic digestion (Wang et al., 2019), catalysts for chemical synthesis and biofuel production (Xiong et al., 2017) or renewable alternatives for rare elements used in electronic appliances (e.g., supercapacitors, Jiang

* Corresponding author.
E-mail address: Kimmo.rasa@luke.fi (K. Rasa).

https://doi.org/10.1016/j.indcrop.2021.113475
Received 2 December 2020; Received in revised form 18 March 2021; Accepted 25 March 2021
Available online 3 April 2021

et al., 2013).

It is well known that biochar chemical properties vary depending on the raw material, processing technology and the processing conditions used (e.g., peak temperature and heating rate) (Gutiérrez et al., 2021; Lin et al., 2019; Zhao et al., 2018). The same also applies to biochar physical properties, but variations in biochar pore properties on different length scales are not completely understood. Gray et al. (2014) presented a conceptual model of biochar pore structure where the biochar internal porosity can be roughly divided into two distinct length scales. The pores measurable on the nanometre-scale are of pyrogenic origin, while larger micrometre-scale pores reflect inherent cellular structures of the raw material. These two pore regimes represent distinct functionalities in biochar applications. Therefore, the intended biochar application determines the most beneficial pore properties of biochar to be used.

In agronomic applications, micrometre-scale pores are responsible for water transport within biochar, and their size distribution is directly reflected in the soil (Rasa et al., 2018) or growing medium water retention properties (Turunen et al., 2020). Accordingly, the size distribution and continuity of micrometre-scale pores regulates the accessibility of fluids and solutes to nanometre-scale pores (i.e., "sorption sites") located inside the biochar skeleton structure (Caguiat et al., 2018; Jiang et al., 2013; Siipola et al., 2018). The micrometre-scale biochar skeleton structure also determines the total volume available for pyrogenic nanopore formation (Gray et al., 2014), and the same applies to nanopores generated via chemical activation. In practise, Qiu et al. (2018) activated biochar with potassium hydroxide and used it as supercapacitor electrode material. They found that after 10 000 charge/discharge cycles in Na_2SO_4 electrolyte both micrometre-scale skeleton structure inherent from biochar raw material properties and nanometre-scale pores originating from activation procedure were still visible.

The inherent micrometre-scale skeleton structure of biochar cannot be modified by a simple adjustment of the pyrolysis temperature, which address the role of raw material selection (Gray et al., 2014; Hyväluoma et al., 2018b). Despite the fundamental role of the skeleton structure in numerous biochar applications, the quantitative data available is still limited. For the first time, the present work quantitatively studies how clonal and within three variation affects to biochar skeleton structure, which is prerequisite for production of homogenous biochar in industrial scale.

In the present study, the recent developments in X-ray microtomography (μCT) and image analysis method (Brodersen, 2013; Cochard et al., 2015; Jyske et al., 2016) have been harnessed to quantitatively study the micrometre-scale pore structure of raw materials and pyrolysis products. The imaging resolution of μCT covers the range required for analysis of wood structural properties (Suuronen and Jyske, 2019) and biochar skeleton structure (Hyväluoma et al., 2018a). Biochar production could also benefit from easy-to-use methods allowing screening of feedstock structural properties and variation. Fibre analysis techniques are traditionally used in the pulp and paper industry to analyse wood structural properties, but whether this approach could be used to predict biochar structural properties prior to pyrolysis is not known.

In this study, we focused on the porous structures of wood and biochar of hybrids of narrow-leaf willow (*S. schwerinii* E.L. Wolf). Willows were chosen as an example due to their vast geographical distribution and existing plantations established during past bioenergy programmes in EU areas. They are deciduous tree species with well-defined structural properties that vary greatly between different species and clones (Sennerby-Forsse, 1989; Monteoliva et al., 2007). The μCT imaging data allow for representative volumetric analysis of wood vessels and fibres, as well as porous structures in biochar, along with 3D visualization of the structural features relevant for targeted biochar applications (Hyväluoma et al., 2018a). Thus, the selected approach probes the biochar fundamental structural properties determined by plant physiology. In the case of willow biochars produced with slow pyrolysis at the temperatures below + 500 °C, specific surface area is low (< 10 m^2 g^{-1}, Rasa et al., 2018), which indicate weakly developed nanometre-scale porosity and dominance of the larger pores.

Five hybrid willow clones were selected for the study. The following aspects of willow wood and derived biochars were studied: 1) clonal, between-sprout, and within-sprout variation in vessel and fibre properties; 2) 3D pore volumes of wood and the corresponding biochar of selected willow clones; and 3) the possibility of predicting biochar structural properties based on conventional fibre analysis conducted for fresh willow material. We hypothesized that the clonal variation in wood characteristics exceeds that of within-sprout variation and that pyrolysis modifies greatly pore dimensions of the raw material. This knowledge allows optimization of biochar structural properties for targeted high value-added applications by facilitating plantation of new willow stands using clones with desired pore properties and/or by selecting the most suitable feedstock from existing short rotation coppice willow stands.

2. Materials and methods

2.1. Willow wood materials

The wood material for the study was collected from a willow clone archive (no 206) located in southwestern Finland at the Preitilä field station (60°27'N, 22°44'E) of the Natural Resources Institute Finland. The archive included willow species hybrids produced by controlled crossings during an energy willow hybridization programme carried out in the 1980s at the Finnish Forest Research Institute. The archive was planted in 2001 and cut down to rejuvenate the coppice in spring 2013.

For this study, five hybrid willow clones were selected (Appendix Table A.1 in Supplementary materials). All the selected clones were by origin hybrids of narrow-leaf willow (*Salix schwerinii,* clone U8955) female parent, with the following four clones as male parents: E4856 *S.* cv. Aquatica, E6748 *S. myrsinifolia*, E6736 *S. phylicifolia* and V7514 *S. viminalis* x *S. dasyclados*. Based on the results of former field trials, the clones selected for this study represented both fast- and slow-growing families (Viherä-Aarnio, 1991).

2.2. Sample collection and measurements of willow sprouts

For the analysis of wood structure and fibre properties, one 5-year-old sample sprout was harvested from three different stools (Appendix Table A.2 in Supplementary materials) of each clone in January 2018. Sprouts of different sizes were selected for the sample (excluding the smallest depressed twigs). The sample sprouts were cut at a height of 5−10 cm from the main stool. Before cutting the sprouts, the outside of the stem basal curve was marked. The height of the sample sprouts as well as the diameters over bark at 60 cm distance from the base and at 150 cm distance from the top were measured (Appendix Table A.3 in Supplementary materials).

A 10-cm-long stem sample was cut between heights of 50–60 cm from the base of the sprout for 3D imaging and between heights of 60–70 cm for fibre analysis (Appendix Fig. A1 in Supplementary materials). Another 10-cm-long sample for 3D imaging and fibre analysis was taken at a 150–160 cm distance from the top of the sprout. The sampling was fixed to the abovementioned heights to avoid possible reaction wood at the base curve of the stem. The top end and the outside curve of the stem samples (in relation to the stool) were marked with a sharp knife to later trace the possible reaction wood and to select comparable samples for the analysis. A bulk sample (approximately 1 kg fresh weight) for pyrolysis was formed by cutting the rest of the sample sprout into 30–50-cm-long pieces up to a diameter of 2 cm. The samples were packed into plastic bags and stored at −20 °C until further processing. The number of sprouts of the sampled stools was counted, and the dominant height and diameter of the five tallest sprouts of each stool were measured.

2.3. Preparation of specimens for structural analysis of wood and biochar

For the measurements of fibre and vessel properties, stem specimens were manually prepared in the laboratory (Fig. 1). The number of sample clones analysed and the locations of specimens within willow sprouts are shown in Table 1. First, the annual rings of stem sections were counted, and their radial widths were measured to an accuracy of the nearest 0.01 mm. The tree-ring measuring equipment consisted of a microscope connected to a computer.

2.3.1. Preparation for porosity analysis of wood and biochar

For the porosity analysis of wood and biochar, smaller specimens were manually excised from the other half of the stem sample (Fig. 1). First, a radial wedge was prepared, and then the 1st and 3rd annual rings (as counted from the bark inwards in the stem disc) of each wedge were cut into two parts for (1) porosity analysis of non-pyrolyzed wood and (2) biochar production and further analysis of biochar porosity (Fig. 1). Excised samples had overall dimensions of 1 mm x 1 mm x 10 mm, and they were dried at 40 °C for 48 h. One sample half was directly used for 3D imaging of wood, while the other half was first directed to slow pyrolysis, and the resulting biochar was then used for 3D imaging (Fig. 1).

2.3.2. Fibre analysis of wood

For the measurements of fibre properties (i.e., fibre length and width), one 3-cm-thick wedge was sawed along the radius of each sample disc (Fig. 1). Then, the wedge was split into two equal parts (1 and 2 in Fig. 1). The inner part contained half of the stem pith. The outer part excluded the cambial zone and bark. The parts were further split into small sticks and macerated in a solution of glacial acetic acid and 50 % hydrogen peroxide (1:1, v/v) at 60 °C for over two nights (modified from Franklin, 1945). Suspensions of washed cells were prepared for fibre analyser measurements by diluting them in water and gently mixing with Bamix (by using a de-sharpened mixing stem). Fibre properties (e.g., length, width) were measured from the specimens by using a standard fibre analysis programme of the Valmet Fibre Image Analyser with Tappi T271-12 and ISO 16065-N standards (FS5; Valmet Automation Oy, Kajaani, Finland). The following measurements were performed: Lc(n), arithmetic mean fibre length, calculated from the population distribution of fibre lengths; Lc(l), length-weighted fibre length, i.e., average mean fibre length measured from a fibre distribution weighted according to the TAPPI T271 standards; Lc(w), weight-weighted average mean fibre length measured from a fibre distribution weighted according to the TAPPI T271 standards; and fibre width, measured as an integral value from the middle of the fibre to account for the tapered fibre ends.

Table 1
Vertical and radial locations and willow clones used for fibre analysis and 3D imaging of wood and biochar. Three parallel sprouts per clone and sample location were used.

Sample	Analysis			
Vertical	Base		Top	
	Fibre, fresh wood			
Radial	Inner[a]	Outer[b]	Inner	Outer
Clones	1–5	1–5	1–5	1–5
	Porosity, dried wood			
Radial	Ring 1[c]	Ring 3[d]	Ring 1	Ring 3
Clones	1,3,5	1,3,5	1,3,5	–
	Porosity, biochar			
Radial	Ring 1	Ring 3	Ring 1	Ring 3
Clones	1,3,5	1,3,5	1,3,5	–

[a] Inner is the inner stem section used for fibre analysis containing half of the stem pith (see Fig. 1).
[b] Outer is the outer stem section used for fibre analysis excluding the cambial zone and bark.
[c] The outermost annual ring as counted from the bark inwards (i.e., year 2017).
[d] The third ring as counted from the bark inwards (i.e., year 2015).

2.4. Biochar production by slow pyrolysis

For pyrolysis, two types of willow samples were prepared: bulk samples for yield analysis and traceable samples for image analysis. For the bulk samples, willow stems (clone no. 5, sprouts 1–3) were cut into slices using a circular saw. For the traceable image analysis, sample slices were excised from each clone-sprout-base/top-combination as described earlier (Fig. 1). One of the excised halves of the sample was stored for image analysis (wood), and the other half was pyrolyzed to produce biochar for image analysis.

For pyrolysis of wood material, bench-scale batch-type pyrolysis equipment was used. The equipment consists of a programmable indirect heating oven, an airtight pyrolysis vessel with an internal temperature measurement system (inside the vessel, sensor TCC-K-250-6.0-KY), a water-jacket cooling system and a gas collection line (gas bag). The pyrolysis vessel was filled with bulk willow wood sample (dry weight 280 g). Each traceable willow sample was placed into a ceramic crucible (individually), and crucibles were buried into the top-most layer of the bulk sample. Thus, we tried to mimic pyrolysis circumstances within bulk samples and simultaneously ensure that samples used in image analyses could be identified. Overall, two batches were pyrolyzed, i.e., 560 g of bulk sample and 18 ceramic crucibles, each containing one individual sample for image analysis. Before pyrolysis, the system was flushed with excess N_2 to remove air. During pyrolysis, the temperature was raised at a rate of 1.7 °C min^{-1} and maintained at + 462 ± 2 °C for 60 min. After cooling, the biochar and tar fractions were weighed, and the volume of gas was determined by using a gas meter

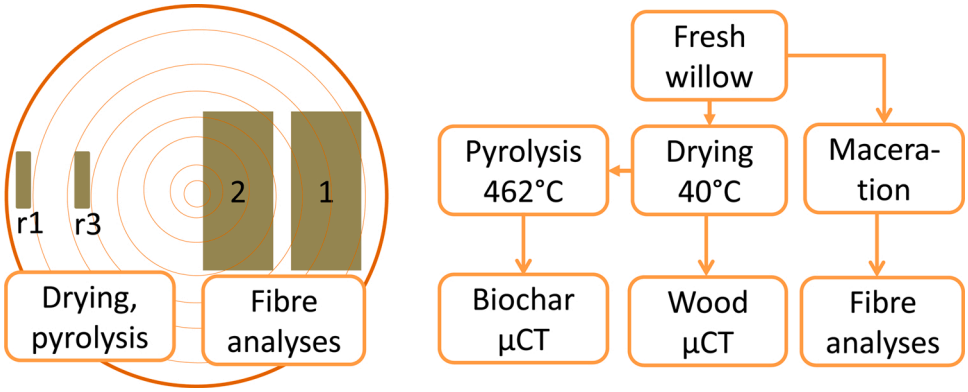

Fig. 1. Process of willow sample preparation for structural analysis of wood and biochar. On the left, r1 is the outermost annual ring counted from the bark inwards (ring 1), r3 is the third ring counted from the bark inwards (ring 3), 1 is the outer stem section used for fibre analysis excluding the cambial zone and bark, and 2 is the inner stem section used for fibre analysis containing half of the stem pith. On the right, schematic presentation of sample pre-treatments before X-ray microtomography (µCT) and fibre analysis.

(Ritter). The traceable biochar samples were used for 3D analysis of porosity.

2.5. X-ray imaging of wood and biochar

For the analysis of wood and biochar porosity, specimens were prepared as described earlier. Each specimen (i.e., clone-sprout-base/top–combination of wood and biochar) was analysed in 3D by using an X-ray microtomography device (μCT) at 1-μm resolution (GE Phoenix Nanotom®, Wunstorf, Germany). Specimens were imaged at a full 360 degrees, resulting in altogether 1000 projections by using a source voltage of 50 kV and a source current of 450 μA. The resulting pixel size was 1 μm by using 2 × 2 binning. The exposure time used was 10 × 500 ms. The sample distance to the radiation source was 3 mm, and the sensor distance to the source was 300 mm. Imaging of one sample took approximately 1½ hours. The resulting projection series were reconstructed into 3D-image stacks by using GE Phoenix datos|x-software. These 3D-image stacks had a voxel size of 1 μm.

2.6. Image processing

Image processing of the reconstructed 3D-image stacks was performed by using FIJI software (Schindelin et al., 2012; Rueden et al., 2017; ImageJ 2.0.0-rc-68/1.54e). The noise levels of our 3D-image stacks were lowered by using anisotropic filtering (Tschmperlé and Deriche, 2005) with edge detecting algorithms (Canny, 1986). Filtered images were converted into binary images using the IJ_isodata algorithm (Ridler and Calvard, 1978), and morphological opening operations were conducted on these images using a 3-dimensional ball element with a diameter of 3 voxels (Legland et al., 2016).

2.7. Image analysis

After image processing, 3D-image stacks were analysed for porosity and 3D pore size distribution of the samples. Porosity is defined as the fraction of the pore volume over the total volume (dimensionless quantity ranging from 0 to 1). Pore size distribution was determined by using the FIJI Xlib-library's pore size distribution plugin. This method starts filling the digital sample with spheres of increasing size until all pore structures have been filled and the maximum size of the spheres has been reached. The methods and macro used in image processing and analysis are described in detail in the Appendix A. Supplementary data (page 2).

2.8. Statistical analysis

The statistical analysis of the porosity differences between wood and biochar, as well as between and within clones of willows, was carried out by using the GLIMMIX procedure of the SAS Enterprise Guide 7.15 (SAS Institute Inc., Cary, NC, USA). The statistical analysis of clonal and within-clone variations in fibre properties was performed by using generalized linear mixed models with the assumptions of beta (with a logit link) and Gaussian (with an identity link) distributions. The first was used when the dependent variable was measured as a percentage. Clones (1, 3 and 5), samples (dried wood and pyrolyzed), and their interactions were used as fixed effects. The location information (top, base, inner and outer) was also included as a fixed effect. Correlated measurements of locations and samples within the same sprout were taken into account in R-side and G-side random effects with compound symmetry covariance structures, respectively.

Generalized linear mixed models with a beta distribution was fitted by using the residual pseudo-likelihood estimation method, and all others were fitted with the restricted maximum likelihood. The residuals were plotted against the fitted values, which indicated that the assumption of normality was met. Pairwise comparisons of means were analysed using the stepdown method of Westfall (Westfall, 1997) with a significance level of $\alpha = 0.05$. The degrees of freedom were calculated using the Kenward–Roger method (Kenward and Roger, 2009).

3. Results and discussion

3.1. Bimodal pore system of willow wood

The total porosity, pore size distribution and visual outlook of imaged samples prior to and after pyrolysis represent typical features of deciduous trees with bimodal pore size distributions (Table 2, Figs. 2 and 3). Bimodal pore size distribution arises from the structure of willow wood (i.e., xylem), which is primarily composed of water conducting vessel elements and fibres that are the bulk of the xylem, providing mechanical support for the trunk. Willow vessel elements are organized in a diffuse-porous tree ring structure with average diameters of approx. 60−80 μm (Sennerby-Forsse, 1989; Cobas et al., 2013). Mature vessels are dead cells with rigid, lignified secondary walls (Hacke and Sperry, 2001). In our study, pores attributed to vessels formed pipe-like structures, as shown in Fig. 3. They had a mean diameter of 42–53 μm (Table 2), but those diameters accounted for only the pore area (lumen, not cell walls). No clear clonal differences in vessel peak diameters were detected, although the pores of clones 3 and 5 were slightly larger than those in clone 1 ($p = 0.061$ and 0.101, respectively). Instead, there was within-sprout variation in the vessel peak diameter depending on the sampling location. The diameter of fibres was larger in the outer part of the base than in the inner part of the base ($p = 0.002$) or top of the sprout ($p < 0.001$).

The lower end of the bimodal pore size distribution is attributed to willow fibres. Based on the literature, the average diameter in willow wood, including the dimensions of the cell lumen and double cell walls, is approx. 13−20 μm (Sennerby-Forsse, 1989, 1985; Monteoliva et al., 2007; Cobas et al., 2013). Our X-ray tomography data show the fibre peak diameter to be approximately 6–8 μm, but as in the case of vessels, those diameters account for only the pore area (lumen, not cell walls). Lumen diameters of approx. 7−14 μm and cell wall thicknesses of approx. 2−4 μm have been reported for willow fibres (Sennerby-Forsse, 1989; Deka et al., 1994; Monteoliva et al., 2007; Cobas et al., 2013). Our data do not indicate clonal differences in the fibre width for samples prior to pyrolysis (Table 2 and Fig. 4), although variation in fibre cell dimensions between willow clones has been reported earlier (e.g., Monteoliva et al., 2007).

Other wood structures, e.g., parenchyma cells storing reserve compounds and rays transporting water in the horizontal direction, can also be distinguished in X-ray tomography figures. Due to resolution limitations, parenchyma cells are not visualized in Fig. 4. Typically, the rays are uniseriate (one row), and the size of the parenchyma falls between the size of fibres and vessels (Karp, 2014). However, their contribution to the total porosity of willow wood and its pore size distribution is minor compared to the dominating vessel- and fibre-related structures. Overall, image analysis data show that there is variation in the willow

Table 2
Total porosity of dried wood and pyrolyzed samples, fraction of pore volumes associated with fibres and vessels to the total porosity (relative pore volume, fibre, vessel) and peak diameter of fibres and vessels (μm, location of pore size maxima, see Fig. 2). For each clone, X-ray tomography data received from different sprouts and locations are pooled. Values with the same letter do not differ statistically at the level of $p < 0.05$.

	Total	Relative pore volume		Peak diameter	
Sample	porosity	Fibre	Vessel	Fibre	Vessel
Clone 1 wood	0.57ab	0.65a	0.35a	6.9	42.0a
Clone 3 wood	0.61b	0.66a	0.34a	7.8	52.9a
Clone 5 wood	0.55a	0.73b	0.27b	6.0	43.6a
Clone 1 pyrol.	0.62b	0.62a	0.38a	6.0	26.5b
Clone 3 pyrol.	0.61b	0.65a	0.35a	6.0	31.2b
Clone 5 pyrol.	0.59ab	0.72b	0.28b	6.0	31.4b

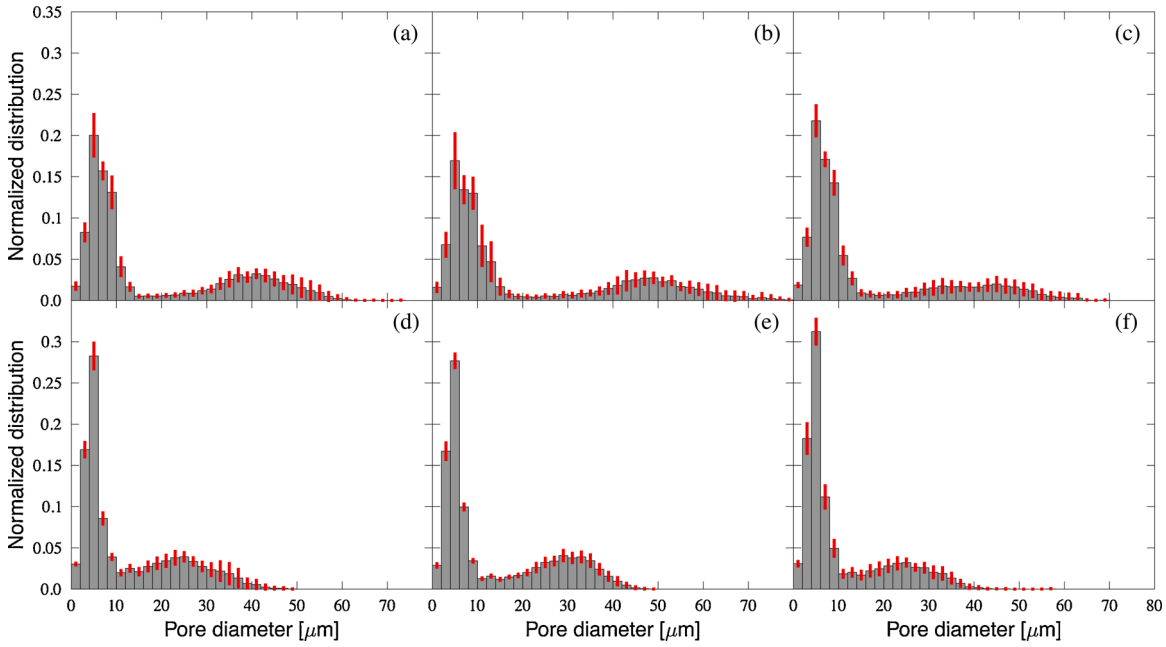

Fig. 2. Pore size distribution of samples prior to (a–c) and after pyrolysis (d–f). Clone 1 in the left column, clone 3 in the middle and clone 5 in the right column. Data from sprouts and locations are pooled, and red bars represent the standard deviation. Note that due to the data being pooled, peak diameters in these distributions are not exactly identical to those given in Table 2.

structural properties between the clones, but variation in some pore characteristics can also occur within the selected clone. The results suggest that willow cultivations growing specific clones could provide rather homogenous raw material sources for biochar production, and by selecting specific parts (top or base) for pyrolysis, the within-clone variation can be further reduced. However, whether harvesting of selected specific parts can be done in practise, remains open.

3.2. *Biochar pore system – effect of pyrolysis*

The total porosity of biochars either remained the same or increased slightly compared to that of raw materials (Table 2). During pyrolysis, 72 % of the sample mass was lost as volatilized gases (data not shown), and wood samples visually shrank during the process. Simultaneous material loss and the change in sample volume levelled off the clonal differences in the total porosity observed for the willow clones prior to pyrolysis. Thus, the total porosities of the produced biochars were equal (Table 2). In contrast, the clonal differences in porosity due to vessel- and fibre-related pores remained before and after pyrolysis (Table 2, clone 5 differs from clones 1 and 3).

The pyrolysis process clearly alters pore dimensions compared to non-pyrolyzed samples. The most remarkable effect of pyrolysis on the pore space characteristics was observed in the mean diameter of fibre- and vessel-related pores. The original diameters of the vessels in the raw materials were 42−53 μm, while in the pyrolysis process, they shrank by almost 50 % (Table 2). Visual inspection also reveals that the shape of the pores flattened (Fig. 3). Similar changes in the cross-sectional shape of both vessel- and fibre-related pores of willow biochar were observed and quantified by Hyväluoma et al. (2018b). Fibre-related pores also shrank, but the change was less drastic. In this study, the shrinkage of sample pieces was not qualitatively measured. The rate of shrinkage depends to some extent on the peak temperature of the pyrolysis process (Hyväluoma et al., 2018b). Caguiat et al. (2018) reported a 21–22 % change in the length of poplar, black locust and pine samples pyrolyzed at 1000 °C. Thus, shrinkage greatly alters both the pore characteristics and particle size of the produced biochars.

Overall, pores associated with fibres form approximately two-thirds of the total porosity of biochars, whereas the rest of the porosity is due to vessel-related pores (Table 2, Fig. 3). The pyrolysis levels off the differences observed in the raw material porosity to some extent, but the major characteristics remain identifiable. It is worth to address that previous helium ion microscopy studies conducted with willow biochars produced in pyrolysis temperature below 500 °C suggest that pores in submicrometre size range are not present in the pore walls indicating that mass loss in pyrolysis mainly occur at sub-nanometre length scale (Hyväluoma et al., 2018b). Lack of nanoscale pores is in line with the low specific surface area of such biochars (Rasa et al., 2018). The most drastic impact of pyrolysis was the shrinkage of wood, which reduced the mean diameters of pores, especially larger pores related to vessel structures. The practical impact of this shrinkage phenomenon might be relevant, for example, in biochar applications related to growing media, where the size of the biochar pores directly affects how strongly water is retained in biochar pores (Rasa et al., 2018; Turunen et al., 2020).

3.3. *Prediction of biochar structural properties*

The relationships between feedstock, pyrolysis process parameters and biochar physicochemical properties (e.g., elemental composition, ash content, pH and specific surface area) have been traditionally established using data synthesis and meta-analysis approaches (Li et al., 2019). However, due to the limited quantitative data available, the prediction of biochar micrometre-scale structure (based on the feedstock used) is not yet possible. Thus, it would be tempting to predict the biochar pore structure by utilizing readily available low-cost research methods used to analyse the properties of wood materials. Therefore, willow fibre properties were analysed using a fibre analyser typically used in the pulp and paper industries and wood science. Compared to μCT-based approach fibre analysis would be 10–50 times cheaper approach (rough estimation based on realized costs of the current study).

The data showed that there was no significant difference in fibre width between the clones (Fig. 3a). The lack of variation between clones is in line with the equal fibre peak diameters detected by X-ray tomography and image analysis (Table 2). Fibre analysis revealed that the fibre width did not depend on the vertical sample location (top or bottom of sprout, Appendix Table A.4 in Supplementary materials), which

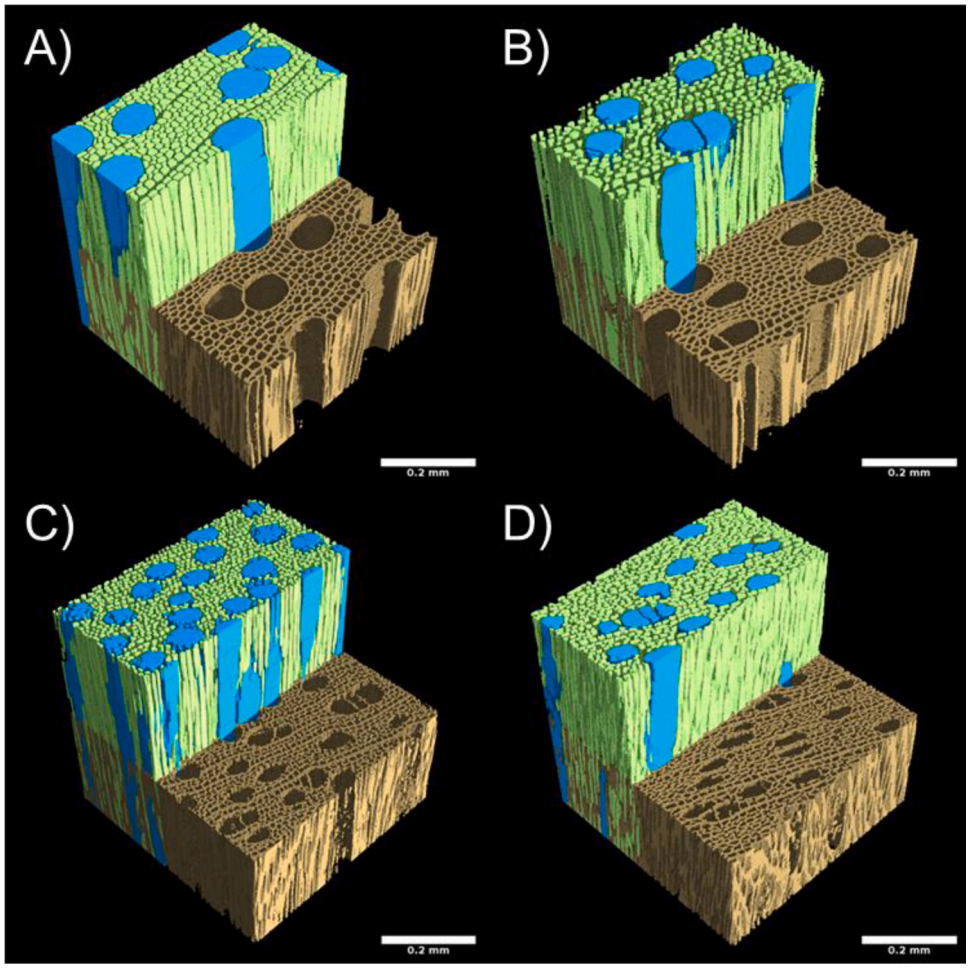

Fig. 3. Typical μCT images of the xylem of the non-pyrolyzed (A, B) and pyrolyzed (C, D) willows. Images A and C represent the porosity in the fast-growing willow clone (3), and images B and D show the porosity in the slow-growing clone (5). Lumens of vessel elements are visualized as blue, and lumens of fibres and parenchyma are visualized as green segments. Brown colour refers to cell wall structures. Bars = 0.2 mm.

suggests that harvesting of entire sprout does not challenge the homogeneity of the raw material. Instead, when observed radially (cross sectional), fibre size differs between the inner and outer parts of the sprout (Appendix Table A.4 in Supplementary materials). These radial differences in fibre dimensions, determined by factors such as cambial age, growth rate, and allometry, cannot be controlled by harvesting strategy. However, as discussed above, pyrolysis tended to level off raw material-dependent structural variation.

The fibre analysis indicated that the mean average width of fresh willow fibres was 12.5 ± 0.39 μm (Fig. 3A), while peak diameters measured by image analysis were between 6 and 8 μm for prior pyrolysis and approximately 6 μm for biochars. The mean size of fibres measured with two different methods is somewhat distinct, but as discussed above, image analysis does not account for the thickness of the cell wall. In addition, samples for image analysis were dried, which likely shrank the samples. Although it is not straightforward, it could be worth studying in detail whether the relationship between fibre analysis and biochar pore dimensions could be established. Other predictive approaches have also been proposed earlier. Wood density has been suggested as an easily measurable proxy for wood cell structure, which in turn could be used to predict plant available water in biochar in soil amendment use (Werdin et al., 2020). In that study, wood density was shown to negatively correlate with plant available water in biochar, i.e., the lower the wood density is, the more void spaces there are available for water in biochar. In wood basic density, significant variation has also been reported among different willow species and clones (Sennerby-Forsse, 1985; Mosseler et al., 1988; Gupta et al., 2014).

To summarize, fibre analysis can be used to pre-assess the homogeneity of biochar raw material sources. This evaluation can be facilitated by scientific knowledge of wood growth- and clone-related factors affecting the structural properties of willows. Thus, it could be possible to select specific well-known raw materials as precursors for biochars with desired pore properties. For future consideration, the latest fibre analysis devices are capable of measuring vessel width, which could improve the usefulness of this technology to predict biochar physical quality.

3.4. Length of willow fibres

According to the literature, willow fibres (0.5−1 mm) are slightly longer than vessel elements (0.4 mm) on average, and a clonal variation exists (Sennerby-Forsse, 1989; Deka et al., 1994; Monteoliva et al., 2007; Gupta et al., 2014). In our study, only fibre length was measured (Fig. 4B). The arithmetic mean fibre length varied from 0.41 mm (Lc(n)) to 0.51 mm (Lc(l)) to 0.57 mm (Lc(w)). For statistical analysis, only the results of Lc(n) were used (typical parameter for scientific purposes). No clonal differences in fibre length were found (Fig. 4, Appendix Table A4 in Supplementary materials), although clone 3 had a slightly (14 %) longer mean fibre length than the other clones (Fig. 4B). The fibres were significantly longer (22 %) in the outer radial location (higher cambial age) than in the inner part of the sprout (Appendix Table A4 in Supplementary materials). The fibres in the stem base were also longer (25

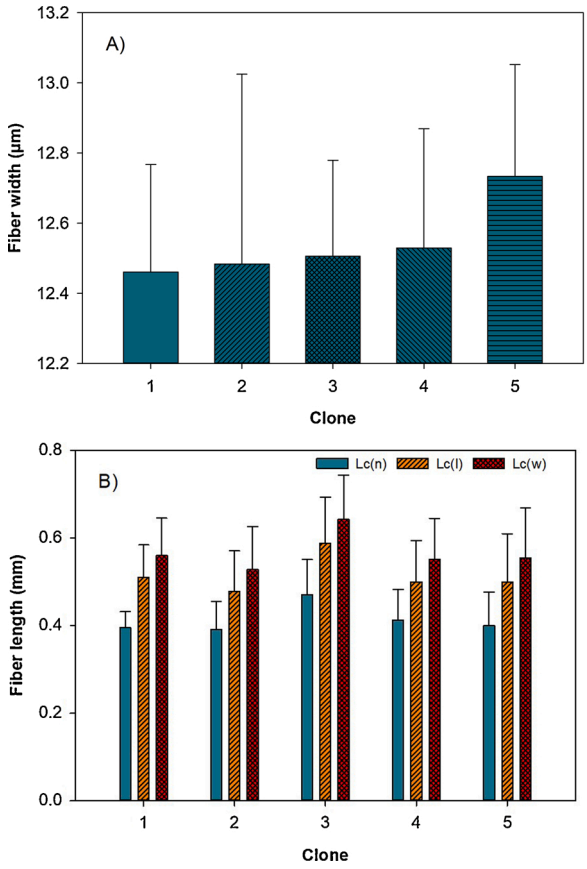

Fig. 4. Variation in average mean fibre width (A) and fibre length (B) between willow hybrids (mean ± SD). To illustrate clonal differences, all samples per clone were pooled together.

%) than the fibres in the top of the sprout stem (Appendix Table A4 in Supplementary materials). The most plausible way to control fibre length is to use either the stem base or the top of the sprout for biochar production. Whether this selection has a practical impact on biochar functionality in different applications is not known. However, long tubular pores more likely provide a continuous pathway through biochar particles, while shorter pores tend to face a dead end. Thus, it is well justified to expect that fibre and vessel lengths versus the particle size of biochar determine the continuity of pores. Whether this assumption is correct and what its practical impacts are on different biochar applications is recommended to be a subject for further studies.

3.5. *Willow cultivations as a source of well-defined biochars*

In the EU, short rotation coppice (SRC) willows have been commercially planted to a significant extent in the past, mainly for energy use purposes. Willows could offer advantages over coniferous tree species due to their fast growth and high productivity. SRC willows could also provide environmental benefits in terms of CO_2 sequestration when grown on marginal sites such as abandoned agricultural or peatlands (Rytter et al., 2015). In Finland, bioenergy-focused projects in the 1980s produced knowledge on the hybridization, cultivation, and management of SRC willows for energy purposes. High biomass yields are achievable if cultivation is based on well-adapted, selected clones and biotic and abiotic damages are avoided (Volk et al., 2004; Verwijst et al., 2013). This existing knowledge can now be used for producing biomass for applications with higher added value.

As shown above, the pore characteristics of biochar can be controlled by carefully selecting the raw material. In the case of willow, monoclonal plantations producing the same clone might be a sufficient solution in practice but harvesting strategy can be adjusted if degree of homogeneity needs to be increased. In Nordic countries, industrial use of forest biomass typically relies on three tree species (spruce, pine and birch), yielding timber and pulp and paper as end-products. Thus, an increase in the selection of tree species and technologies used in biomass processing could create new value-chains and improve resource efficiency if mainstreamed. Willows used in this experiment act as an example species, demonstrating that biochar porosity can largely be controlled in short rotation cultivation when big amounts of homogenous biochars are needed for designed high-added value applications. Extending the present approach to other raw materials would enable production of applicable biochars to be used as carbon precursor materials for range of applications. As addressed also elsewhere (e.g. Liu et al., 2019), there is need for deeper and systemic understanding how biochar pore structure throughout the length-scales (from sub-nanometre to micrometre) affect biochar performance in different applications.

From economical perspective, production of homogenous biochar as precursor for activated carbons used in high value-added applications could be feasible option compared to traditional use of biochar in agriculture, where payback time of the investment is long (Maroušek et al., 2019) and benefits for farmers are unsure (Soinne et al., 2020). Tailored biochars with well-defined structural properties are an example of bio-based materials that could be further modified and used in various energy storage and conversion applications (Liu et al., 2019). For example, global market of the supercapacitors is expected to exceed $\$100 \times 10^9$ after 2020 (Huang et al., 2019). In addition, a recent techno-economic analyses of combined energy and activated carbon production (biochar as intermediate product) suggest that integrated production systems may have a great economical potential (Liu et al., 2021).

4. Conclusions

Biochar micrometre-scale pore properties are strongly and directly dependent on the inherent structural properties of the raw material used. This skeletal structure regulates biochar functionality in all applications relying on the porous structure of biochar. Previous studies have shown that biochar skeleton structure varies greatly between different biochar types. Our study shows quantitatively that the source of variation in biochar pore structure can be controlled and predicted to a large extent by knowing and selecting the wood material used in biochar production. The selection can be performed at the required accuracy relevant for intended biochar application. In the case of willow, monoclonal plantations provide homogenous raw material, yielding biochar with an even pore structure. Readily available and inexpensive-to-use fibre analysis techniques can be used to estimate adequate homogeneity of raw material sources. Willow was used as an example case due to existing plantations across Europe, and the results suggest that new valuable value-chains for short rotation coppices could be established. The approach used in the study could be extended to other raw materials, which would facilitate the control of physical quality of produced biochar.

Funding

The authors gratefully acknowledge Luke's strategic financing for the project titled 'More, faster, higher quality: potential of short-rotation aspen and willow biomass for novel products in bioeconomy' (AspenWill) and the Ministry of Education and Culture, Finland, project Bioproduct and Clean Bioeconomy – RDI FlagShip in Xamk.

CRediT authorship contribution statement

Kimmo Rasa: Conceptualization, Methodology, Validation, Investigation, Writing - original draft, Writing - review & editing, Funding

acquisition. **Anneli Viherä-Aarnio:** Resources, Investigation, Writing - original draft, Writing - review & editing. **Peetu Rytkönen:** Methodology, Validation, Investigation, Writing - review & editing, Visualization. **Jari Hyväluoma:** Methodology, Validation, Investigation, Writing - original draft, Writing - review & editing, Visualization. **Janne Kaseva:** Methodology, Formal analysis, Writing - original draft, Writing - review & editing. **Heikki Suhonen:** Methodology, Writing - review & editing, Visualization. **Tuula Jyske:** Conceptualization, Methodology, Validation, Writing - original draft, Writing - review & editing, Supervision, Project administration, Funding acquisition.

Declaration of Competing Interest

The authors declare that they have no known competing financial interests or personal relationships that could have appeared to influence the work reported in this paper.

Acknowledgements

The authors would like to acknowledge the support of Esa Ek, Elvi Pääkkönen and Kalle Kaipanen for skilful assistance with the field and laboratory work, and Johanna Nikama for conducting pyrolysis experiments.

Appendix A. Supplementary data

Supplementary material related to this article can be found, in the online version, at doi:https://doi.org/10.1016/j.indcrop.2021.113475.

References

Bartoli, M., Giorcelli, M., Jagdale, P., Rovere, M., Tagliaferro, A., 2020. A review of non-soil biochar applications. Material 13, 261. https://doi.org/10.3390/ma13020261.

Brassard, P., Godbout, S., Raghavan, V., 2016. Soil biochar amendment as a climate change mitigation tool: key parameters and mechanisms involved. J. Environ. Manage. 181, 484–497. https://doi.org/10.1016/j.jenvman.2016.06.063.

Brodersen, C.R., 2013. Visualizing wood anatomy in three dimensions with high-resolution X-ray micro-tomography (μCT)—a review. IAWA J. 34, 408–424. https://doi.org/10.1163/22941932-00000033.

Caguiat, J.N., Yanchus, D.S., Gabhi, R.S., Kirk, D.W., Jia, C.Q., 2018. Identifying the structures retained when transforming wood in biocarbon. J. Anal. Appl. Pyrol. 136, 77–86. https://doi.org/10.1016/j.jaap.2018.10.020.

Canny, J., 1986. A computational approach to Edge detection. IEEE T. Pattern Anal. PAMI-8,6, pp. 679–698. https://doi.org/10.1109/TPAMI.1986.4767851.

Cobas, A.C., Felissia, F.E., Monteoliva, S., Area, M.C., 2013. Optimization of the properties of poplar and willow chemimechanical pulps by a mixture design of juvenile and mature wood. BioResources 8, 1646–1656. https://doi.org/10.15376/biores.8.2.1646-1656.

Cochard, H., Delzon, S., Badel, E., 2015. X-ray microtomography (micro-CT): a reference technology for high-resolution quantification of xylem embolism in trees. Plant Cell Environ. 38, 201–206. https://doi.org/10.1111/pce.12391.

Deka, G.C., Wong, B.M., Roy, D.N., 1994. Variation of specific gravity, fibre length and cell wall thickness in young Salix clones. J. Wood Chem. Technol. 14, 147–158.

Franklin, G.L., 1945. Preparation of thin sections of synthetic resins and wood-resin composites, and a new macerating method for wood. Nature (London) 155, 51. https://doi.org/10.1038/155051a0.

Gray, M., Johnson, M.G., Dragila, M.I., Kleber, M., 2014. Water uptake in biochars: the roles of porosity and hydrophobicity. Biomass Bioenergy 61, 196–205. https://doi.org/10.1016/j.biombioe.2013.12.010.

Gupta, A., Singh, N.B., Choudhary, P., Sharma, J.P., Sankhayan, H.P., 2014. Estimation of genetic variability, heritability and genetic gain for wood density and fibre length in 36 clones of white willow (Salix alba L.). Int. J. Agric. Environ. Biotechnol. 7, 299–304. https://doi.org/10.5958/2230-732X.2014.00247.2.

Gutiérrez, J., Rubio-Clemente, A., Pérez, J.F., 2021. Effect of main solid biomass commodities of patula pine on biochar properties produced under gasification conditions. Ind. Crops Prod. 160, 1–16. https://doi.org/10.1016/j.indcrop.2020.113123.

Hacke, U.G., Sperry, J.S., 2001. Functional and ecological xylem anatomy. Perspectives in Plant Ecology, Evolution and Systematics 4, 97–115. https://doi.org/10.1078/1433-8319-00017.

Huang, S., Zhu, X., Sarkar, S., Zhao, Y., 2019. Challenges and opportunities for supercapacitors. APL Mater. 7, 100901 https://doi.org/10.1063/1.5116146.

Hyväluoma, J., Kulju, S., Hannula, M., Wikberg, H., Källi, A., Rasa, K., 2018a. Quantitative characterization of pore structure of several biochars with 3D imaging. Environ. Sci. Pollut. Res. 25, 25648–25658. https://doi.org/10.1007/s11356-017-8823-x.

Hyväluoma, J., Hannula, M., Arstila, K., Wang, H., Kulju, S., Rasa, K., 2018b. Effects of pyrolysis temperature on the hydrologically relevant porosity of willow biochar. J. Anal. Appl. Pyrol. 134, 446–453. https://doi.org/10.1016/j.jaap.2018.07.011.

Jiang, J., Wang, X., Holm, N., Rajagopalan, K., Chen, F., Ma, S., 2013. Highly ordered microporous woody biochar with ultra-high carbon content as supercapacitor electrodes. Electrochim. acta. 113, 481–489.

Jyske, T., Kuroda, K., Suuronen, J.-P., Pranovich, A., Roig Juan, S., Aoki, D., Fukushima, K., 2016. In planta localization of stilbenes within Picea abies phloem. Plant Physiol. 172, 913–928. https://doi.org/10.1104/pp.16.00990.

Karp, A., 2014. Willows as a source of renewable fuels and diverse products. In: Fenning, T. (Ed.), Challenges and Opportunities for the World's Forests in the 21st Century. Forestry Sciences, vol. 81. Springer, Dordrecht.

Kenward, M.G., Roger, J.H., 2009. An improved approximation to the precision of fixed effects from restricted maximum likelihood. Comput. Stat. Data Anal. 53, 2583–2595. https://doi.org/10.1016/j.csda.2008.12.013.

Legland, D., Arganda-Carreras, I., Andrey, P., 2016. MorphoLibJ: integrated library and plugins for mathematical morphology with ImageJ. Bioinformatics (Oxford Univ. Press) 32 (22), 3532–3534. https://doi.org/10.1093/bioinformatics/btw413. PMID 27412086 (on Google Scholar).

Lehmann, J., Rillig, M.C., Thies, J., Masiello, C.A., Hockaday, W.C., Crowley, D., 2011. Biochar effects on soil biota - a review. Soil Biol. Biochem. 43, 1812–1836. https://doi.org/10.1016/j.soilbio.2011.04.022.

Li, S., Harris, S., Anandhi, A., Chen, G., 2019. Predicting biochar properties and functions based on feedstock and pyrolysis temperature: a review and data syntheses. J. Clean Prod. 255, 890–902. https://doi.org/10.1016/j.jclepro.2019.01.106.

Lin, B.-J., Silveira, E.A., Colin, B., Chen, W.-H., Lin, Y.-Y., Leconte, F., Pétrissans, A., Rousset, P., Pétrissans, M., 2019. Modeling and prediction of devolatilization and elemental composition of wood during mild pyrolysis in a pilot-scale reactor. Ind. Crops Prod. 131, 357–370.

Liu, W.-J.-, Jiang, H., Yu, H.-Q., 2019. Emerging applications of biochar-based materials for energy storage and conversion. Energy Environ. Sci. 12, 1751–1779. https://doi.org/10.1039/c9ee00206e.

Liu, L., Qian, H., Mu, L., Wu, J., Feng, X., Lu, X., Zhu, J., 2021. Techno-economic analysis of biomass processing with dual outputs of energy and activated carbon. Bioresour. Technol. 319, 124108 https://doi.org/10.1016/j.biortech.2020.124108.

Monteoliva, S., Area, M.C., Felissia, F.E., 2007. CMP pulps of willows for newsprint. I. Pulp evaluation. Cell. Chem. Technol. 41, 263–272.

Mosseler, A., Zsuffa, L., Stoehr, M.U., Kenney, W.A., 1988. Variation in biomass production, moisture content, and specific gravity in some North American willows (Salix L.). Can. J. Forest Res. 18, 1535–1540. https://doi.org/10.1139/x88-235.

Qiu, Z., Wang, Y., Bi, X., Zhou, T., Zhou, J., Zhao, J., Miao, Z., Yi, W., Peng Fu, P., Zhuo, S., 2018. Biochar-based carbons with hierarchical micro-meso-macro porosity for high rate and long cycle life supercapacitors. J. Power Sources 376, 82–90. https://doi.org/10.1016/j.jpowsour.2017.11.077.

Rasa, K., Heikkinen, J., Hannula, M., Arstila, K., Kulju, S., Hyväluoma, J., 2018. How and why does willow biochar increase a clay soil water retention? Biomass Bioenergy 119, 346–353. https://doi.org/10.1016/j.biombioe.2018.10.004.

Ridler, T.W., Calvard, S., 1978. Picture thresholding using an iterative selection method. IEEE T. Syst. Man Cyb. 8, 630–632. https://doi.org/10.1109/TSMC.1978.4310039.

Rueden, C.T., Schindelin, J., Hiner, M.C., Dezonia, B.E., Walter, A.E., Arena, E.T., Eliceiri, K.W., 2017. ImageJ2: imageJ for the next generation of scientific image data. BMC Bioinf. 18, 529. https://doi.org/10.1186/s12859-017-1934-z.

Rytter, R.-M., Rytter, L., Högbom, L., 2015. Carbon sequestration in willow (Salix spp.) plantations on former arable land estimated by repeated field sampling and C budget calculation. Biomass Bioenergy 83 (2015), 483–492.

Schindelin, J., Arganda-Carreras, I., Frise, E., et al., 2012. Fiji: an open-source platform for biological-image analysis. Nat. Methods 9, 676–682. https://doi.org/10.1038/nmeth.2019.

Sennerby-Forsse, L., 1985. Clonal variation of wood specific gravity, moisture content, and stem bark percentage in 1-year-old shoots of 20 fast-growing Salix clones. Can. J. For. Res. 15, 531–534. https://doi.org/10.1139/x85-087.

Sennerby-Forsse, L., 1989. Wood structure and quality in natural stands of Salix caprea and Salix pentandra L. Stud. Forestalia Suecica 182, 1–17.

Siipola, V., Tamminen, T., Källi, A., Lahti, R., Romar, H., Rasa, K., Keskinen, R., Hyväluoma, J., Hannula, M., Wikberg, H., 2018. Effects of biomass type, carbonization process, and activation method on the properties of bio-based activated carbons. BioResources 13, 5976–6002. https://doi.org/10.15376/biores.13.3.5976-6002.

Soinne, H., Keskinen, R., Heikkinen, J., Hyväluoma, J., Uusitalo, R., Peltoniemi, K., Velmala, S., Pennanen, T., Fritze, H., Kaseva, J., Hannula, M., Rasa, K., 2020. Are there environmental or agricultural benefits in using forest residue biochar in boreal agricultural clay soil? Sci. Total Environ. 731. https://doi.org/10.1016/j.scitotenv.2020.138955.

Suuronen, J.-P., Jyske, T., 2019. Noninvasive investigation of phloem structure by 3D synchrotron X-ray microtomography. In: Johannes, Liesche (Ed.), Phloem - Methods and Protocols. Humana, New York, NY, pp. 37–54. https://doi.org/10.1007/978-1-4939-9562-2_4. Methods in Molecular Biology. 2014.

Tschmperlé, D., Deriche, R., 2005. Vector-valued image regularization with PDE's: a common framework for different applications. IEEE Trans. Pat. Anal. Mach. Intell. 27, 506–517.

Turunen, M., Hyväluoma, J., Heikkinen, J., Keskinen, R., Kaseva, J., Hannula, M., Rasa, K., 2020. Quantifying the pore structure of different biochars and their impacts on the water retention properties of Sphagnum moss growing media. Biosyst. Eng. 191, 96–106. https://doi.org/10.1016/j.biosystemseng.2020.01.006.

Verwijst, T., Lundkvist, A., Edelfeldt, S., Albertsson, J., 2013. Development of sustainable willow short rotation forestry in Northern Europe. In: Matovic, M.D. (Ed.), Biomass Now – Sustainable Growth and Use. IntechOpen. https://doi.org/10.5772/55072.

Viherä-Aarnio, A., 1991. Overview of willow (Salix spp. L) Breeding in Finland. Reports from the Foundation for Forest Tree Breeding, 1, pp. 81–86.

Volk, T.A., Verwijst, T., Tharakan, P.J., Abrahamson, L.P., White, E.H., 2004. Growing fuel: a sustainability assessment of willow biomass crops. Front. Ecol. Environ. 2, 411–418. https://doi.org/10.1890/1540-9295(2004)002[0411:GFASAO]2.0.CO;2.

Wang, G., Li, Q., Gao, X., Wang, X.C., 2019. Sawdust-derived biochar much mitigates VFAs accumulation and improves microbial activities to enhance methane production in thermophilic anaerobic digestion. ACS Sustain. Chem. Eng. 7, 2141–2150. https://doi.org/10.1021/acssuschemeng.8b04789.

Werdin, J., Fletcher, T.D., Rayner, J.P., Williams, N.S.G., Farrell, C., 2020. Biochar made from low density wood has greater plant available water than biochar made from high density wood. Sci. Total Environ. 705, 135856 https://doi.org/10.1016/j.scitotenv.2019.135856.

Westfall, P.H., 1997. Multiple testing of general contrasts using logical constraints and correlations. J. Am. Stat. Assoc. 92, 299–306. https://doi.org/10.2307/2291474.

Xiong, X., Yu, I.K.M., Cao, L., Tsang, D.C.W., Zhang, S., Ok, Y.S., 2017. A review of biochar catalyst for chemical synthesis, biofuel production and pollution control. Bioresour. Technol. 246, 254–270. https://doi.org/10.1016/j.biortech.2017.06.163.

Zhao, B., O'Connor, D., Zhang, J., Peng, T., Shen, Z., Tsang, D.C.W., Hou, D., 2018. Effect of pyrolysis temperature, heating rate, and residence time on rapeseed stem derived biochar. J. Clean. Prod. 174, 977–987. https://doi.org/10.1016/j.jclepro.2017.11.013.